J Stat Phys (2010) 138: 815–837
DOI 10.1007/s10955-009-9901-3

Pattern Formation in Growing Sandpiles with Multiple Sources or Sinks

Tridib Sadhu · Deepak Dhar

Received: 17 September 2009 / Accepted: 30 November 2009 / Published online: 10 December 2009

Abstract Adding sand grains at a single site in the Abelian sandpile models produces beautiful but complex patterns. We study the effect of sink sites on such patterns. Sinks change the scaling of the diameter of the pattern with the number N of sand grains added. For example, in two dimensions, in the presence of a sink site, the diameter of the pattern grows as $\sqrt{(N/\log N)}$ for large N, whereas it grows as $\sqrt{N}$ if there are no sink sites. In the presence of a line of sink sites, this rate reduces to $N^{1/3}$. We determine the growth rates for various sink geometries along with the case when there are two lines of sink sites forming a wedge, and generalizations to higher dimensions. We characterize the asymptotic pattern in the large N limit for one such case, the two-dimensional F-lattice with a single source adjacent to a line of sink sites. The characterization is done in terms of the positions of different spatial features in the pattern. For this lattice, we also provide an exact characterization of the pattern with two sources, when the line joining them is along one of the axes of the lattice.

Keywords Pattern formation · Self-organized criticality

1 Introduction

It is well known that beautiful and complex patterns can be generated by the deterministic evolution of systems under simple local rules, e.g. in the Game of life [1], and Turing patterns [2]. Sandpiles, on a flat table with boundaries, formed by adding sand grains at a constant rate, gives rise to singular structures like ridges in the stationary state, which have attracted much attention recently [3, 4]. In the Abelian sandpile model (ASM), growing sandpiles produce richer and hence more interesting patterns. This model is inspired by real

T. Sadhu (✉) · D. Dhar
Department of Theoretical Physics, Tata Institute of Fundamental Research, Homi Bhaba Road, Mumbai 400005, India
e-mail: tridib@theory.tifr.res.in

D. Dhar
e-mail: ddhar@theory.tifr.res.in

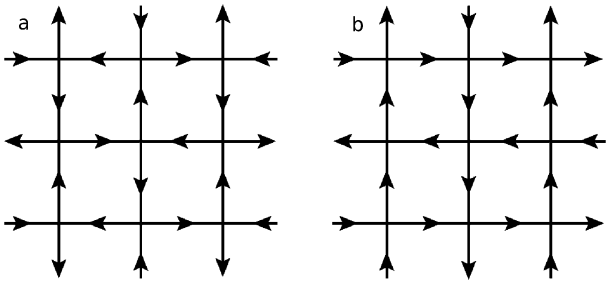

Fig. 1 The lattices studied in this paper: (**a**) F-lattice and (**b**) Manhattan lattice

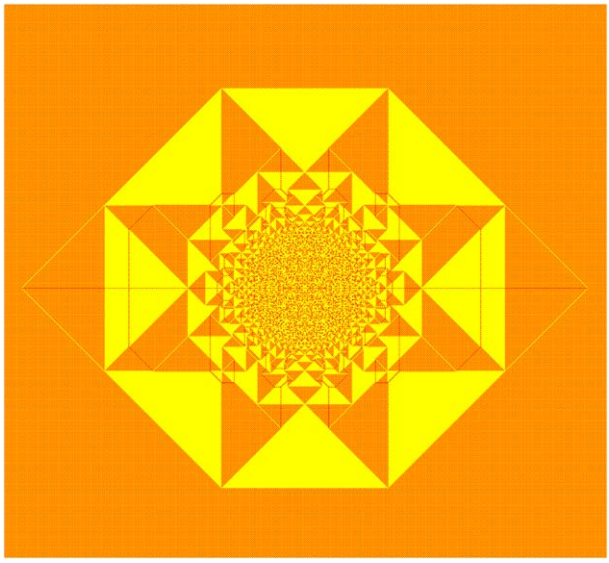

Fig. 2 (Color online) Stable configuration for the ASM, obtained by adding 5×10^4 grains at one site, on the F-lattice of Fig. 1(a) with initial checkerboard configuration. Color code: *red* = 0, *yellow* = 1. Apparent *orange regions* in the picture represent patches with checkerboard configuration. (Details can be seen in the online version using zoom in)

sandpile dynamics, but has different rules of evolution. The steady state of sandpile models with slow driving, in the presence of a boundary, has been much studied in the context of self-organized criticality [5]. The Abelian sandpile model, with particles added at one site, on an infinite lattice with periodic particle distribution has the very interesting property of *proportionate growth* [6]. This is a well-known feature of the biological growth in animals, where different parts of the growing animal grow at roughly the same rate. Our interest in studying growing sandpiles comes from this being the prototypical model of proportionate growth. Most of the other growth models studied in the physics literature, such as diffusion-limited aggregation, or surface deposition, do not show this property. In these models, growth is confined to some active outer region. The inner structures, once formed are frozen in and do not evolve further in time [7].

In [6], we studied growing sandpiles in the Abelian model on the F-lattice and the Manhattan lattice. These are directed variants of the square lattice, obtained by assigning directions to the bonds, as shown in Fig. 1. We found that for three different choices of the initial background configuration, the same pattern is produced (Fig. 2). We were able to characterize this pattern exactly. One of these special initial configurations is the one in which each alternate site of the lattice is occupied, forming a checkerboard pattern. If we add particles at the origin, and relax the configuration using the sandpile toppling rule, we generate a beautiful, but fairly complex pattern, made up of triangles and dart-shaped regions (called

"patches" (Fig. 2)), that shows proportionate growth and an unexpected 8-fold rotational symmetry. The full characterization of this pattern reveals an interesting underlying mathematical structure, which seems to deserve further exploration. This is what we do in the present paper by adding sink sites or multiple sources.

The presence of sink sites changes the pattern in interesting ways. In particular, it changes how different spatial lengths in the pattern scale with the number of added grains N. For example, in the absence of sink sites, the diameter of the pattern grows as $\sqrt{N}$ for large N, whereas in the presence of a single sink site, this changes to a $\sqrt{N/\log N}$ growth. If there is a line of sink sites next to the site of addition, the growth rate is $N^{1/3}$. We also study the case in which the source site is at the corner of a wedge-shaped region of wedge angle ω, where the wedge boundaries are absorbing. We show that for any ω the pattern grows as N^{α}, with $\alpha = \omega/(\pi + 2\omega)$. This analysis is extended to other lattices with different initial height distributions, and to higher dimensions.

We also studied the exact characterization of the asymptotic pattern in the infinite N limit for the pattern with a line of sink sites. For a single point source, the determination of the different distances in the pattern requires a solution of the Laplace equation on a discrete Riemann surface of two-sheets [6]. Interestingly, for the pattern with a line sink, we still have to solve the discrete Laplace equation, but the structure of the Riemann surface changes from two-sheets to three-sheets.

We study the effect on the pattern of having multiple sites of addition. For multiple sources, the pattern of small patches near each source is not substantially different from a single-source pattern, but some rearrangements occur in the larger outer patches. Two patches may sometimes join into one, or, conversely, a patch may break up into two. While the number of patches undergoing such changes is finite, the sizes and positions of all the patches are affected by the presence of the other source, and we show how these changes can be calculated exactly for the asymptotic pattern.

Spatial patterns in the sandpile models were first discussed by Liu et al. [8]. The asymptotic shape of the boundaries of the sandpile patterns produced by adding grains at a single site in different periodic backgrounds was discussed in [9]. Borgne et al. [10] obtained bounds on the rate of growth of these boundaries and later these bounds were improved by Fey et al. [11] and Levine et al. [12]. The first detailed analysis of different periodic structures found in the patterns were carried out by Ostojic in [13, 14]. Other spatial configurations in the Abelian sandpile models, like the identity [10, 15, 16] or the stable state produced from special unstable states, show complex internal self-similar structures [8], which also share common features with the patterns studied here. There are other models, which are related to the Abelian sandpile model, e.g. the Internal Diffusion-Limited Aggregation (IDLA), Eulerian walkers (also called the rotor-router model), and the infinitely-divisible sandpile, which also show similar structure. For the IDLA, Gravner and Quastel showed that the asymptotic shape of the growth pattern is related to the classical Stefan problem in hydrodynamics, and determined the exact radius of the pattern with a single point source [17]. Levine and Peres have studied patterns with multiple sources in these models recently, and proved the existence of a limit shape [18].

This paper is organized as follows. We define the model in Sect. 2, and briefly recapitulate the main ideas in the analysis of the single source pattern. Then, in Sect. 3, we discuss scaling the of the diameter of the patterns with N for different sink geometries. First, we consider the pattern in the presence of a line of sink sites. Then, this analysis is extended to other sink geometries: two intersecting line sinks in two dimensions and two or three intersecting planes of sink sites in three dimensions. The problem of a single sink site is a bit different from the others, and is discussed separately in Sect. 4. In Sect. 5, we numerically verify the

growth rates. The remaining sections are devoted to a detailed characterization of some of these patterns. In Sect. 6, we characterize the pattern in the presence of a line sink. In Sect. 7, we discuss the case when there are two sources present. These analytical calculations of the metric properties of the asymptotic pattern are compared in Sect. 8, with the measured values for the patterns with finite but large N. Section 9, contains a summary and some concluding remarks.

2 The Single Source Pattern

We consider the Abelian sandpile model on the F-lattice (Fig. 1a). This is a square lattice with directed bonds such that each site has two inward and two outward arrows. A different assignment of the arrow directions, that gives us the Manhattan lattice is shown in Fig. 1b. The asymptotic pattern formed by the growing sandpile on the Manhattan lattice is the same as that on the F-lattice [6]. We shall discuss here only the F-lattice, but the discussion is equally applicable to the Manhattan lattice.

Define a position vector on the lattice, $\mathbf{R} \equiv (x, y)$. In the Abelian sandpile model, a height variable $z(\mathbf{R})$, called the number of grains on the site, is assigned to each site $\mathbf{R}$. In a stable configuration all sites have height $z(\mathbf{R}) < 2$. The system is driven by adding grains at a single site and if this addition makes the system unstable it relaxes by the toppling rule: each unstable site transfers one grain each in the direction of its outward arrows. We start with an initial checkerboard configuration in which $z(\mathbf{R}) = 1$ for sites with $(x + y) =$ even, and 0 otherwise. Clearly, the average density of sand grains for the initial configuration is $1/2$ per site. For numerical purpose we used a lattice large enough so that none of the avalanches reaches the boundary. The result of adding $N = 5 \times 10^4$ grains at the origin is shown in Fig. 2.

The characterization of this pattern in the large-N limit is discussed in detail in [6]. Define $2\Lambda(N)$ as the diameter of a pattern, when N grains have been added, measured as the height of the smallest rectangle that encloses all sites that have toppled at least once. As mentioned before, the pattern exhibits proportionate growth. While there is as yet no rigorous proof of this important property, we assume this in the following. Then, it is natural to describe the pattern in the reduced coordinates defined by $\xi = x/\Lambda$ and $\eta = y/\Lambda$. A position vector in these reduced coordinates is defined by $\mathbf{r} = \mathbf{R}/\Lambda \equiv (\xi, \eta)$. Then in the limit $\Lambda \to \infty$, the pattern can be characterized by a function $\rho(\mathbf{r})$ which gives the local density of sand grains in a small rectangle of size $\delta\xi\delta\eta$ about the point $\mathbf{r}$, with $1/\Lambda \ll \delta\xi, \delta\eta \ll 1$. We define $\Delta\rho(\mathbf{r})$ as the change in density $\rho(\mathbf{r})$ from its initial background value. The pattern is made of a union of distinct regions, called "Patches", where $\Delta\rho(\mathbf{r})$ is constant inside each patch and takes only two possible values, $1/2$ in a high-density patch (color yellow in Fig. 2) and 0 in a low-density patch (color orange).

Let $T_\Lambda(\mathbf{R})$ be the number of topplings at site the $\mathbf{R}$ when the diameter reaches the value 2Λ for the first time. Define

$$\phi(\mathbf{r}) = \lim_{\Lambda\to\infty} \frac{1}{2\Lambda^2} T_\Lambda(\mathbf{R}'), \tag{1}$$

where $\mathbf{R}' \equiv (\lfloor \Lambda\xi \rfloor, \lfloor \Lambda\eta \rfloor)$, with $\lfloor x \rfloor$ being the floor function which gives the largest integer $\leq x$. From the conservation of sand-grains in the toppling process, it is easy to see that ϕ satisfies the Poisson equation [6]

$$\nabla^2\phi(\mathbf{r}) = \Delta\rho(\mathbf{r}) - \frac{N}{\Lambda^2}\delta(\mathbf{r}). \tag{2}$$

The complete specification of $\phi(\mathbf{r})$ determines the density function $\Delta\rho(\mathbf{r})$ which in turn characterizes the asymptotic pattern. The condition that determines $\phi(\mathbf{r})$ is the requirement that inside each patch of constant density, it is a quadratic function of ξ and η [6]. Let us write

$$\phi(\mathbf{r}) = a\xi^2 + 2h\xi\eta + b\eta^2 + d\xi + e\eta + f, \tag{3}$$

where a, h, b, d, e and f are constants inside a patch and $a + b = \Delta\rho/2$ corresponding to the patch. Then each patch is characterized by the values of these parameters. The continuity of $\phi(\mathbf{r})$ and its derivatives along the boundary between two adjacent patches imposes linear relations among the corresponding parameters. These linear equations can be solved on the adjacency graph of patches which forms a square lattice on a two sheeted Riemann surface [6].

3 Rate of Growth of the Patterns

For the single source pattern, the diameter $2\Lambda(N) \simeq 2\sqrt{N}$, for large N. We want to study how this dependence gets modified in the presence of sink sites.

First, consider the pattern formed by adding sand grains at a single site in the presence of a line of sink sites. Any grain reaching a sink site gets absorbed, and is removed from the system. For simplicity let us consider the source site at $\mathbf{R}_o \equiv (x_o, 0)$ and the sink sites along the y-axis. A picture of the pattern produced by adding 14336000 grains at $(1, 0)$ is shown in Fig. 3.

The equation analogous to (2) for this problem is

$$\nabla^2\phi(\mathbf{r}) = \Delta\rho(\mathbf{r}) - \frac{N}{\Lambda^2}\delta(\mathbf{r} - \mathbf{r}_o), \tag{4}$$

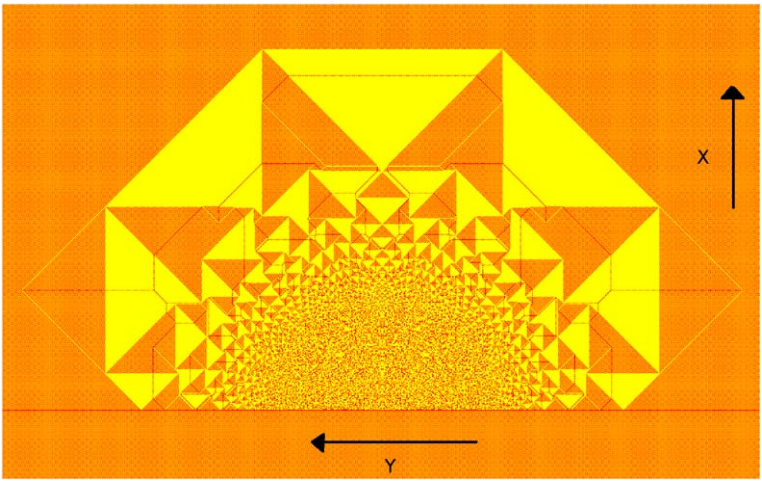

Fig. 3 (Color online) Pattern produced by adding grains at a single site adjacent to a line of sink sites. Color code: *red* = 0 and *yellow* = 1. Apparent *orange regions* in the picture represent patches with checkerboard configuration. (Zoom in for details in the online version.). Note that the pattern is rotated anti-clockwise by 90°

for all $\mathbf{r}$ in the right-half plane with $\xi > 0$, where $\mathbf{r}_o$ is the position of the source in reduced coordinates. Also, as there is no toppling at the sink sites, ϕ must satisfy the boundary condition

$$\phi(\mathbf{r}) = 0 \quad \text{for all } \mathbf{r} \equiv (0, \eta). \tag{5}$$

We can think of ϕ as the potential due to a point charge N/Λ^2 at $\mathbf{r}_o$ and an areal charge density $-\Delta\rho(\mathbf{r})$, in the presence of a grounded conducting line along the η-axis. This problem can be solved using the well-known method of images in electrostatics. Let $\mathbf{r}'$ be the image point of $\mathbf{r}$ with respect to the η-axis. Define $\Delta\rho(\mathbf{r})$ in the left half plane as

$$\Delta\rho(\mathbf{r}') = -\Delta\rho(\mathbf{r}). \tag{6}$$

Then the Poisson equation for this new charge configuration is

$$\nabla^2\phi(\mathbf{r}) = \Delta\rho(\mathbf{r}) - \frac{N}{\Lambda^2}\delta(\mathbf{r} - \mathbf{r}_o) + \frac{N}{\Lambda^2}\delta(\mathbf{r} - \mathbf{r'}_o). \tag{7}$$

As the function $\Delta\rho(\mathbf{r})$ is odd under reflection, ϕ automatically vanishes along the η-axis.

We define N_r as the number of sand grains that remain unabsorbed. Then

$$N_r = \sum_{x>0}\sum_{y} \Delta z(x, y), \tag{8}$$

where $\Delta z(x, y)$ is the change in the height variables between its values before and after the system relaxes. Clearly, for large Λ, we can write

$$N_r \simeq \Lambda^2 \int_{\mathbb{H}} d\tau\, \Delta\rho(\mathbf{r}), \tag{9}$$

where $d\tau = d\xi d\eta$ is the infinitesimal area around $\mathbf{r} \equiv (\xi, \eta)$. The integration is performed over the right half-plane $\mathbb{H}$ with $\xi > 0$. We shall use the sign $\simeq$ to denote equality up to leading order in Λ. Since $\Delta\rho(\mathbf{r})$ is a non-negative bounded function, exactly zero outside a finite region, this integral exists. Let its value be C_2, then we have

$$N_r \simeq C_2\Lambda^2. \tag{10}$$

Let N_a denote the number of grains that are absorbed by the sink sites. Then considering that the grains can reach the sink sites only by toppling at its neighbors we have

$$N_a \simeq \frac{1}{2}\sum_{y} T_\Lambda(1, y). \tag{11}$$

The factor $1/2$ comes from the fact that in the F-lattice, only half of the sites on the column $x = 1$ would have arrows going out to the sink sites. Then using our scaling ansatz in (1), for Λ large,

$$T_\Lambda(1, y) \simeq 2\Lambda \left.\frac{\partial\phi}{\partial\xi}\right|_{\xi=0}. \tag{12}$$

Hence

$$N_a \simeq \Lambda^2 \int_{-\infty}^{\infty} d\eta \left.\frac{\partial\phi}{\partial\xi}\right|_{\xi=0}. \tag{13}$$

Now from (7) the potential ϕ can be written as the sum of two terms: ϕ_{dipole} due to two point charges N/Λ^2 and $-N/\Lambda^2$ at $\mathbf{r}_o \equiv (\xi_o, 0)$ and its image point $\mathbf{r}'_o \equiv (-\xi_o, 0)$ respectively, and the term ϕ_{rest} due to the areal charge density.

$$\phi(\mathbf{r}) = \phi_{dipole}(\mathbf{r}) + \phi_{rest}(\mathbf{r}), \tag{14}$$

where

$$\begin{aligned} \nabla^2\phi_{dipole}(\mathbf{r}) &= -\frac{N}{\Lambda^2}\delta(\mathbf{r}-\mathbf{r}_o) + \frac{N}{\Lambda^2}\delta(\mathbf{r}-\mathbf{r}'_o), \\ \nabla^2\phi_{rest}(\mathbf{r}) &= \Delta\rho(\mathbf{r}). \end{aligned} \tag{15}$$

We first consider the case where R_o is finite and $r_o = R_o/\Lambda$ vanishes in the large Λ limit. Then ϕ_{dipole} reduces to a dipole potential, and it diverges near the origin. However, $\phi_{rest}(\mathbf{r})$ is a continuous and differentiable function for all $\mathbf{r}$. From the solution of the dipole potential, it is easy to show that

$$\phi_{dipole}(r,\theta) = A\frac{\cos\theta}{r}, \tag{16}$$

for $1 \gg r \gg 1/\Lambda$, where we have used polar coordinates (r, θ) with θ being measured with respect to the ξ-axis. Here A is a numerical constant, which is a property of the asymptotic pattern. Then

$$\left.\frac{\partial\phi}{\partial\xi}\right|_{\xi=0} = \frac{A}{\eta^2}, \tag{17}$$

and the integral in (13) diverges as A/η_{min}, where η_{min} is the cutoff introduced by the lattice. Using $\eta_{min} = \mathcal{O}(1/\Lambda)$ it is easy to show that

$$N_a \simeq C_1\Lambda^3, \tag{18}$$

where C_1 is a constant. Then using (10) and (18) and that N_a and N_r add up to N, we get

$$C_1\Lambda^3 + C_2\Lambda^2 \simeq N. \tag{19}$$

Considering the dominant term in the expression for large Λ, it follows that Λ increases as $N^{1/3}$.

For the patterns in the other limit where the source is placed at a distance $\mathcal{O}(\Lambda)$ such that r_o is non-zero for $\Lambda \to \infty$, ϕ_{dipole} is non-singular along the sink line. Then, clearly $N_a \sim \Lambda^2$ and as a result $\Lambda(N) \sim N^{1/2}$.

The above analysis can be easily generalized to a case with the sink sites along two straight lines intersecting at an angle ω and a point source inside the wedge. For a square lattice, $\omega = 0, \pi/2, \pi, 3\pi/2$ and 2π are most easily constructed, and avoid the problems of lines with irrational slopes, or rational numbers slopes with large denominators. The wedge with wedge-angle $\omega = \pi/2$ is obtained by placing the sink sites along the x and y-axis and the source site at $\mathbf{R}_o \equiv (1, 1)$ in the first quadrant. The pattern with a line sink, discussed in previous section, corresponds to $\omega = \pi$.

For the general ω, the corresponding electrostatic problem reduces to determining the potential function ϕ inside a wedge formed by two intersecting grounded conducting lines. Again the potential has two contributions: the potential $\phi_{point}(\mathbf{r})$ due to a point charge at the source site and the potential $\phi_{rest}(\mathbf{r})$ due to the areal charge density. We first consider

the case where the source site is placed at a finite distance from the wedge corner such that the distance in reduced coordinates vanishes in the large Λ limit. In this limit ϕ_{rest} is a non-singular function of $\mathbf{r}$ while ϕ_{point} diverges close to the origin. A simple calculation of the electrostatic problem gives

$$\phi_{point}(r,\theta) \approx A \frac{\sin \alpha\theta}{r^{\alpha}}, \tag{20}$$

where $\alpha = \pi/\omega$ and we have used polar coordinates (r,θ) with the polar angle θ measured from one of the absorbing lines. Again A is a constant independent of N or Λ and is a property of the asymptotic pattern. Then arguing as before, we get

$$N_a \simeq C_1 \Lambda^{2+\alpha} \quad \text{and} \quad N_r \simeq C_2 \Lambda^2. \tag{21}$$

So the equation analogous to (19) is

$$C_1 \Lambda^{2+\alpha} + C_2 \Lambda^2 \simeq N. \tag{22}$$

For wedge angle $\omega = \pi$, $\alpha = 1$, and the above equation reduces to (19).

Similar arguments involving conformal transformation have been used earlier in the context of equilibrium statistical physics to determine the wedge-angle dependence of surface critical exponents near a wedge [19].

For the problem where the source site is at a distance $\mathcal{O}(\Lambda)$ from the wedge corner both the functions ϕ_{rest} and ϕ_{point} are nonsingular close to the origin. It is easy to show that $\Lambda(N)$ grows as $N^{1/2}$.

These arguments can be easily extended to other lattices with different initial height distributions, or to higher dimensions. Consider, for example, an Abelian sandpile model defined on the cubic lattice. The allowed heights are from 0 to 5, and a site topples if the height exceeds 5, and sends one particle to each neighbor. The sites are labelled by the Cartesian coordinates (x, y, z), where x, y and z are integers. We consider the infinite octant defined by $x \geq 0$, $y \geq 0$, $z \geq 0$. We start with all heights equal to 4, and add sand grains at the site $(1, 1, 1)$. We assume that the sites on planes $x = 0$, $y = 0$ and $z = 0$ are all sink sites, and any grain reaching there is lost. We add N grains and determine the diameter of the resulting stable pattern.

We again write the potential function in two parts: ϕ_{point} due to a point charge at $(1/\Lambda, 1/\Lambda, 1/\Lambda)$ and ϕ_{rest} due to the bulk charge density in the presence of three conducting grounded planes. Then, a simple electrostatic calculation shows that the potential ϕ_{point} is the octapolar potential with it's form in spherical polar coordinate as

$$\phi(r,\theta,\Phi) \approx \frac{f(\theta,\phi)}{r^4}. \tag{23}$$

This then implies that the equation determining the dependence of Λ on N is

$$C_1 \Lambda^6 + C_2 \Lambda^3 \simeq N. \tag{24}$$

4 A Single Sink Site

Let the site of addition be the origin, with the sink site placed at $\mathbf{R}_o$. We shall show that when $\mathbf{R}_o$ lies in a high-density patch (color yellow in Fig. 4), the asymptotic patterns are identical to the one produced in the absence of the sink site.

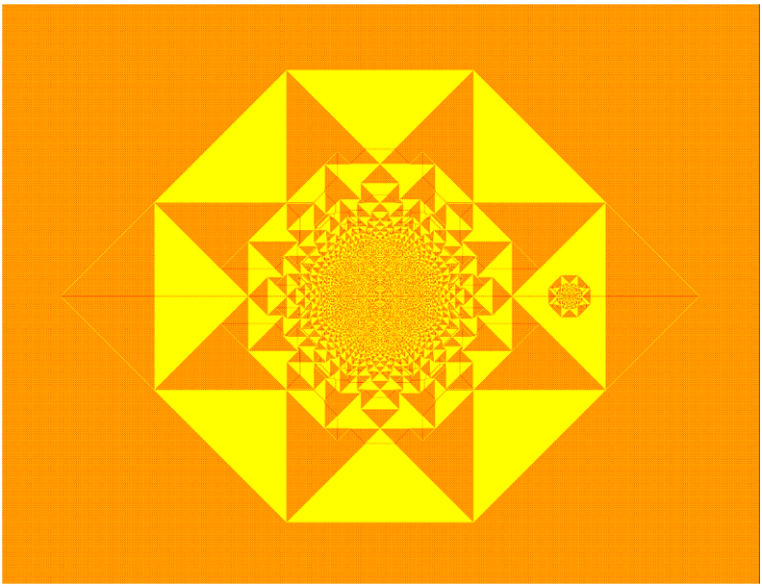

Fig. 4 (Color online) The pattern produced by adding 224000 grains at the origin with a sink site at (400, 0), inside a patch of density 1 (color *yellow*). Color code: *red* = 0 and *yellow* = 1. The apparent orange regions correspond to the checkerboard height distribution. (Zoom in for details in the online version.)

The patterns, produced for r_o close to 1, with the sink sites placed deep inside a high-density patch are simple to analyze, even for finite but large Λ. One such pattern is presented in Fig. 4.

We see that the effect of the sink site on the pattern is to produce a depletion pattern centered at this site. The depletion pattern is a smaller copy of the single source pattern. We define the function $\Delta z_{sink}(\mathbf{R}; N)$ as the difference between the heights at $\mathbf{R}$ in the final stable configuration produced by adding N grains at the origin, with and without the sink site.

$$\Delta z_{sink}(\mathbf{R}; N) = \Delta z_{source+sink}(\mathbf{R}; N) - \Delta z_{source}(\mathbf{R}; N). \tag{25}$$

From the figure it is seen that, in this case, $\Delta z_{sink}(\mathbf{R}; N)$ is the negative of the pattern produced by a smaller source, centered at $\mathbf{R}_0$. The number of grains required to produce this smaller pattern is exactly the number of grains N_a absorbed at the sink site.

$$\Delta z_{sink}(\mathbf{R}; N) = -\Delta z_{source}(\mathbf{R} - \mathbf{R}_o; N_a). \tag{26}$$

This is immediately seen from the fact that the toppling function $T_\Lambda(\mathbf{R})$ satisfies

$$\Delta T_\Lambda(\mathbf{R}) = \Delta z_{source+sink}(\mathbf{R}; N) - N\delta_{\mathbf{R},\mathbf{0}} + N_a\delta_{\mathbf{R},\mathbf{R}_o}, \tag{27}$$

where Δ is the toppling matrix for the sandpile model on the F-lattice [5]. Let $T_{source}(\mathbf{R}; N)$ be the number of topplings at $\mathbf{R}$, when we add N particles at the origin in the absence of any sink site. Since (27) is a linear equation, it follows that a solution of this equation is

$$T_\Lambda(\mathbf{R}) = T_{source}(\mathbf{R}; N) - T_{source}(\mathbf{R} - \mathbf{R}_o; N_a). \tag{28}$$

This is a valid solution for our problem, if the corresponding heights in the final configuration with the sink are all non-negative. This happens when the region with nonzero Δz_{sink} is confined within a high-density patch of the single source pattern.

The number N_a can be determined from the requirement that the number of topplings at the sink site is zero. The potential function for the single source problem diverges as $(4\pi)^{-1}\log r$ near the source [6]. Considering the ultraviolet cutoff due to the lattice, $T_{source}(\mathbf{R}, N)$ at $\mathbf{R} = 0$ can be approximated by $(4\pi)^{-1}N\log N$ to leading order in N. Then at $\mathbf{R} = \mathbf{R}_0$, $T_{source}(\mathbf{R} - \mathbf{R}_o; N_a)$ is approximately equal to $(4\pi)^{-1}N_a \log N_a$ whereas $T_{source}(\mathbf{R}_0; N) \approx N\phi_{source}(\mathbf{r}_0)$, where $\phi_{source}(\mathbf{r})$ is the potential function for the problem without a sink. Then from (28) we have

$$\frac{1}{4\pi}N_a \log N_a \simeq N\phi_{source}(\mathbf{r}_o). \tag{29}$$

For large N, this implies that

$$N_a \simeq 4\pi\phi_{source}(\mathbf{r}_o)N/\log N. \tag{30}$$

Then, in the large N limit, for a sink at a fixed reduced coordinate $\mathbf{r}_o$, the relative size of the defect produced by the sink site decreases as $1/\sqrt{\log N}$. Hence asymptotically, the fractional area of the defect region will decrease to zero, if the sink position $\mathbf{r}_o$ is inside a high-density patch.

When the sink site is inside a low-density patch, the subtraction procedure in (26) gives negative heights, and no longer gives the correct solution. However it is observed for the patches in the outer layer, where the patches are large, that the effect of the sink site is confined within the neighboring high-density patches (Fig. 5) and rest of the pattern in the asymptotic limit remains unaffected.

The pattern in which the source and the sink sites are adjacent to each other, appears to be very similar to the one produced without the sink site. This is easy to see. The Poisson equation analogous to equation (2) for this problem is

$$\nabla^2\phi(\mathbf{r}) = \Delta\rho(\mathbf{r}) - \frac{N}{\Lambda^2}\delta(\mathbf{r}) + \frac{N_a}{\Lambda^2}\delta(\mathbf{r} - \mathbf{r}_o), \tag{31}$$

where N_a is the number of grains absorbed in the sink site at $\mathbf{r}_o$. In an electrostatic analogy, as discussed earlier, ϕ can be considered as the potential due to a distributed charge of density $-\Delta\rho(\mathbf{r}_o)$ and two point charges of strength N/Λ^2 and $-N_a/\Lambda^2$, placed at the origin and at $\mathbf{r}_o$ respectively. It is easy to see that the dominant contribution to the potential is the monopole term with net charge $(N - N_a)/\Lambda^2$. The contribution due to other terms decreases as $1/\Lambda$ for large Λ, and the asymptotic pattern is the same as without a sink, with $N - N_a$ particles added.

The number N_a of particles absorbed is determined by the condition that the number of topplings at $(1, 0)$ (the sink position) is zero. The potential produced at $(1, 0)$ and $(0, 0)$, by the areal charge density is nearly the same. The number of topplings at $(1, 0)$, if we add N_a particles at the sink site, is approximately $(4\pi)^{-1}N_a \log N_a$. Now, from the solution of the discrete Laplacian, the number of topplings produced at $(1, 0)$ due to N particles added at $(0, 0)$ is approximately $(4\pi)^{-1}(N\log N - CN)$ with C being an undetermined constant. Equating these two, we get

$$N_a \log N_a \simeq N\log N - CN. \tag{32}$$

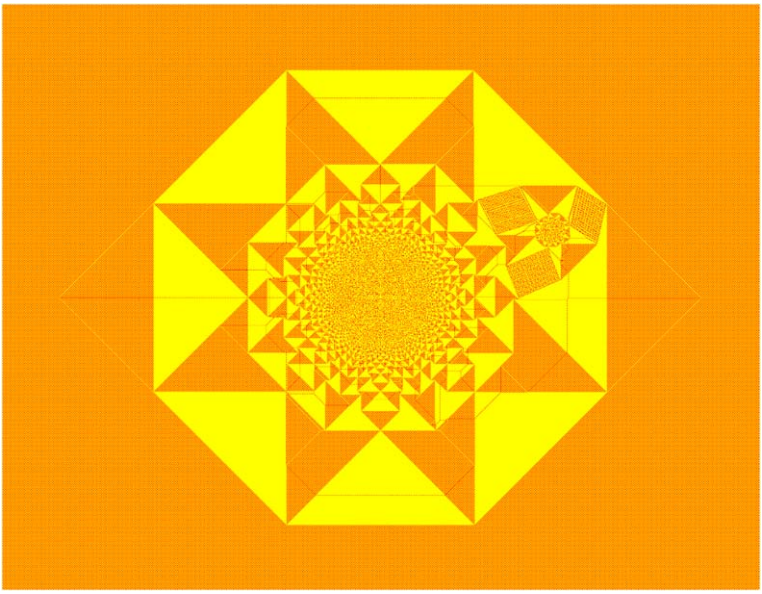

Fig. 5 (Color online) The pattern produced by adding 224000 grains at the origin with a sink site placed at (360, 140), inside a low-density patch. Color code *red* = 0 and *yellow* = 1. The apparent *orange regions* correspond to the checkerboard height distribution. (Details can be seen in the online version using zoom in.)

As the asymptotic pattern is the same as that produced by adding $(N - N_a)$ grains at the origin without a sink, we have $N - N_a \simeq \Lambda^2$, and

$$(N - \Lambda^2)\log(N - \Lambda^2) \simeq N \log N - CN. \tag{33}$$

Simplification of this equation for large N shows that Λ grows as $\sqrt{N/\log N}$ with N.

For finite N, the leading correction to $\phi(\mathbf{r})$ comes from the dipole term in the potential. This term breaks the reflection symmetry of the pattern about the origin. A measure of the bilateral asymmetry is the difference of the boundary distances on two opposite sides of the source. As the relative contribution of the dipole potential compared to the monopole term decays as $\log \Lambda/\Lambda$, for large Λ, this difference vanishes in the asymptotic pattern in the reduced coordinates.

5 Numerical Results

All the above scaling behaviors are verified by the measurement of lengths in the patterns for finite, but large N. Let $\Lambda^*_{line}(N)$ be the real positive root of (19) for a given integer value of N. As Λ_{line} takes only the integer values on the lattice, an estimate of it would be $Nint[\Lambda^*_{line}(N)]$, the integer nearest to $\Lambda^*_{line}(N)$. Interestingly, we found that for a choice of $C_1 = 0.1853$ and $C_2 = 0.528$, this estimate gives values which differ from the measured values at most by 1 for all N in the range of 100 to 3×10^6. We rewrite (19) as

$$0.1853\Lambda^3_{line} + 0.528\Lambda^2_{line} \doteqdot N, \tag{34}$$

where we used the symbol $\doteqdot$ to denote that both sides differ at most by 1. Clearly more precise estimates of C_1 and C_2 would be required if we want this to work for larger N.

Similarly for the other two equations (22) and (24) we find that they are in very good agreement with our numerical data. We consider the case of wedge angle $\omega = 2\pi$. This corresponds to the case with the source site next to an infinite half-line of sink sites. Here $\alpha = 1/2$ and (22) reduces to

$$C_1 \Lambda_{\omega=2\pi}^{5/2} + C_2 \Lambda_{\omega=2\pi}^{2} \simeq N. \tag{35}$$

Choosing $C_1 = 0.863408$ and $C_2 = 0.043311$, we find that the function $Nint[\Lambda^*_{\omega=2\pi}(N)]$ differs from the measured values by at most 1 for all N in the range of 100 to 2×10^5. Then, as in (34), we write

$$0.863408 \Lambda_{\omega=2\pi}^{5/2} + 0.043311 \Lambda_{\omega=2\pi}^{2} \doteqdot N. \tag{36}$$

Similarly, for the three dimensional Abelian sandpile model with the source site inside the first octant and $x = 0$, $y = 0$, and $z = 0$ as the absorbing planes, the equation determining the dependence of the diameter on N is

$$0.0159 \Lambda_{3d}^{6} + 88 \Lambda_{3d}^{3} \doteqdot N. \tag{37}$$

We have verified this equation for N between 5×10^5 to 5×10^8.

We obtained these equations by determining the number of absorbed grains N_a and the remaining grains N_r from dimensional counting grounds, and the final equations are then only a statement of the conservation of the sand grains. It is quite remarkable that this scaling analysis gives almost the exact values of the diameter. In addition, these equations have an important feature that they include a "correction to scaling" term whereas the usual scaling analysis ignores the sub-leading powers.

We also verify (30) using patterns with fixed $\mathbf{r}_o$ and the sink site inside a high-density patch in the outer layer of the pattern. It is found that for a change of N from 224000 to 896000, $N_a \log N/N$ changes by less than 7%, which is consistent with the scaling relation.

In the other limit, where the sink site is next to the source, the dependence of Λ on N is given in (33). We measure $\Lambda(N)$ for the patterns with the sink site at $(1, 0)$ and the source at the origin. For N in the range of 100 to 5×10^5 we find that the function $Nint[\Lambda^*_{point}(N)]$ with $C = 2.190$ in (33), gives almost exact values of $\Lambda(N)$, with their difference being at most 1. Then we write

$$(N - \Lambda_{point}^2) \log(N - \Lambda_{point}^2) \doteqdot N \log N - 2.190N. \tag{38}$$

In the last case, let R_1 and R_2 be the boundary distances measured along the positive and the negative x axis. The difference $R_2 - R_1$ is plotted in Fig. 6 where the data is found to fit to the function $1.22 \log(R_2 + 0.5)$. This confirms the result that the relative bilateral asymmetry $(R_2 - R_1)/R_2$ vanishes in the asymptotic pattern as $\log \Lambda/\Lambda$.

6 Characterization of the Pattern with a Line Sink

The pattern with a line sink (Fig. 3), discussed in Sect. 3, retained two important properties present in the single source pattern (Fig. 2). These are: The asymptotic pattern is made of the union of two types of patches of excess density $1/2$ and 0 and the separating boundaries of the patches are straight lines of slope 0, ± 1 or ∞. However the adjacency graph is changed

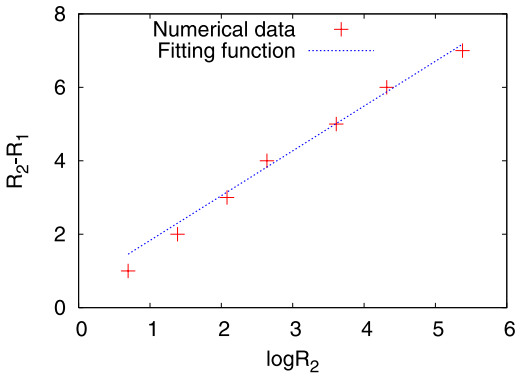

Fig. 6 The bilateral asymmetry due to the presence of a sink site in Fig. 4

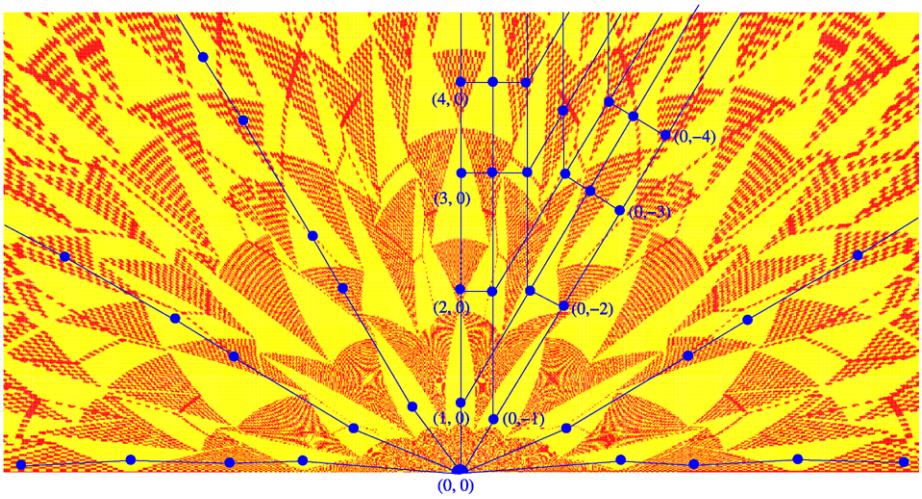

Fig. 7 (Color online) $1/r^3$ transformation of the pattern in Fig. 3. Two adjoining patches are connected by drawing a *straight line*

significantly and this changes the sizes of the patches as well. In this section we show how to explicitly determine the potential function on this adjacency graph.

The adjacency graph of the patches is shown in Fig. 8. This representation of the graph is easier to see by taking the $1/r^3$ transformation of the pattern and then joining neighboring patches by straight lines (Fig.7). Each vertex in the graph is connected to four neighbors except for the vertices corresponding to the patches next to the absorbing line. These have coordination number 3. Also the vertex at the center corresponding to the exterior of the pattern is connected to seven neighbors.

Let us write the quadratic potential function in a patch P having excess density $1/2$ as

$$\phi_P(\mathbf{r}) = \frac{1}{8}(m_P + 1)\xi^2 + \frac{1}{4}n_P\xi\eta + \frac{1}{8}(1 - m_P)\eta^2 + d_P\xi + e_P\eta + f_P, \tag{39}$$

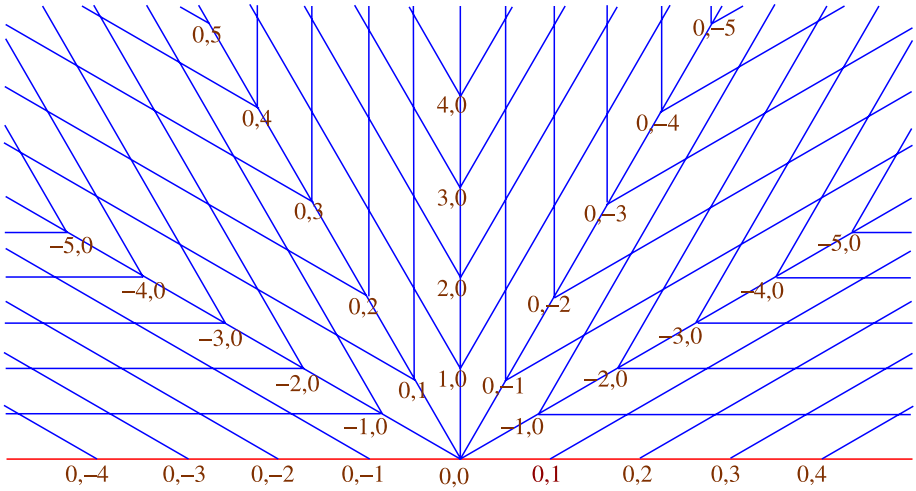

Fig. 8 (Color online) The adjacency graph of the patches corresponding to the pattern in Fig. 3

where the parameters m, n, d, e and f take constant values within a patch. Similarly for a low-density patch P'

$$\phi_{P'}(\mathbf{r}) = \frac{1}{8} m_{P'}(\xi^2 - \eta^2) + \frac{1}{4} n_{P'} \xi\eta + d_{P'}\xi + e_{P'}\eta + f_{P'}. \tag{40}$$

Using the continuity of $\phi(\mathbf{r})$ and its first derivatives along the common boundaries between neighboring patches it has been shown that for the single source pattern without sink sites m, and n take integer values [6]. The same argument also applies to this problem and it can be shown that (m, n) are the coordinates of the patches in the adjacency graph in Fig. 8. These coordinates are shown next to some of the vertices. There are two different patches corresponding to the same set of (m, n) values. In fact, as in the single source pattern the adjacency graph forms a square lattice on a two sheeted Riemann surface, the same is formed for this pattern, but on a three sheeted Riemann surface. This can be constructed by modifying the graph in Fig. 8 keeping its topology the same. In this representation the pattern covers half of the surface with (m, n) being the Cartesian coordinates on the surface.

Define function $D(m, n) = d(m, n) + ie(m, n)$ on this lattice. As discussed in [6], the continuity of $\phi(\mathbf{r})$ and its first derivatives along the common boundary between neighboring patches imposes linear relations between d and e of the corresponding patches. Using these matching conditions it can be shown that d and e satisfy the discrete Cauchy-Riemann conditions [6]

$$\begin{aligned} d(m+1, n+1) - d(m, n) &= e(m, n+1) - e(m+1, n), \\ e(m+1, n+1) - e(m, n) &= d(m+1, n) - d(m, n+1), \end{aligned} \tag{41}$$

and then the function D satisfies the discrete Laplace equation

$$\sum_{i=\pm1} \sum_{j=\pm1} D(m+i, n+j) - 4D(m, n) = 0, \tag{42}$$

on this adjacency graph.

Let us define $M = m + in$ and $z = \xi + i\eta$. As argued before, close to the origin the potential ϕ diverges as $1/r$ (see (16)). Then, the corresponding complex potential function $\Phi(z) \sim 1/z$. As $M \sim d^2\Phi/dz^2$, and $D \sim d\Phi/dz$, it follows that for large $|M|$,

$$D \sim M^{2/3}. \tag{43}$$

Also, the condition that on the absorbing line $\phi(\mathbf{r})$ must vanish implies that for the vertices with even n along the red line in Fig. 8 $e(0, n)$ vanishes. These vertices correspond to the patches with the absorbing line as the horizontal boundary in Fig. 3.

Equation (42) with the above constraint and the boundary condition (see (43)) has a unique solution. The normalization of ϕ is fixed by the requirement that $d(1, 0) = -1$, which fixes the diameter of the pattern to be 2 in reduced units. All the spatial distances in the pattern can be expressed in terms of this solution $D(m, n)$ using the matching conditions between two neighboring patches. As an example, consider the boundary between the patches corresponding to (m, n) and $(m + 1, n)$ with $(m + n)$ being odd. The matching conditions only allow a horizontal boundary between them with the equation $\eta = \eta_p$, where

$$e(m + 1, n) - e(m, n) = \eta_p/2. \tag{44}$$

Similarly there is a vertical boundary between the patches (m, n) and $(m - 1, n)$, with the equation $\xi = \xi_p$, where

$$d(m - 1, n) - d(m, n) = \xi_p/2. \tag{45}$$

The other boundaries can similarly be determined using the solution for $D(m, n)$. The characterization of the asymptotic patterns for $\omega = \pi/2$, $3\pi/2$ and 2π is qualitatively similar and will not be discussed here.

7 Patterns with Two Sources

In this section we discuss patterns produced by adding N grains each at two sites placed at a distance $2\Lambda\mathbf{r_0}$ from each other along the x-axis, at $\Lambda\mathbf{r}_o$ and $-\Lambda\mathbf{r}_o$ with $\mathbf{r}_o \equiv (\xi_o, 0)$. Again, the diameter 2Λ is defined as the height of the smallest rectangle enclosing all sites that have toppled at least once. The two limits, r_0 close to zero and r_0 large are trivial: For $r_o \to 0$, the asymptotic pattern is the same as that produced by adding grains at a single site. On the other hand if $r_o > 1$, each source produces its own pattern, which do not overlap, and the final pattern is a simple superposition of the two patterns.

As noted before, the adjacency graph for the single source pattern has a square lattice structure on a Riemann surface of two-sheets [6]. Then the graph for two non-intersecting single source patterns is a square lattice on two disjoint Riemann surfaces, each having two-sheets (Fig. 11). Only the vertex at the origin represents the exterior of the pattern, which is the same for both of the single source patterns. It has sixteen neighbors and is placed midway between the two Riemann surfaces. For later convenience let us associate the lower Riemann surface to the pattern around the left source at $-\mathbf{r}_o$ and denote it by Γ_L. Similarly the upper Riemann surface as Γ_R corresponding to the pattern around the right source $\mathbf{r}_o$.

For $0 < r_o < 1$, the two single source patterns overlap. Using the Abelian property, we first topple as if the second source were absent. The resulting pattern still has some unstable sites in the region where the patterns overlap. Further relaxing these sites transfers these excess grains outward, and changes the dimensions and positions of the patches: some patches become bigger, some may merge, and sometimes a patch may beak into two disjoint patches.

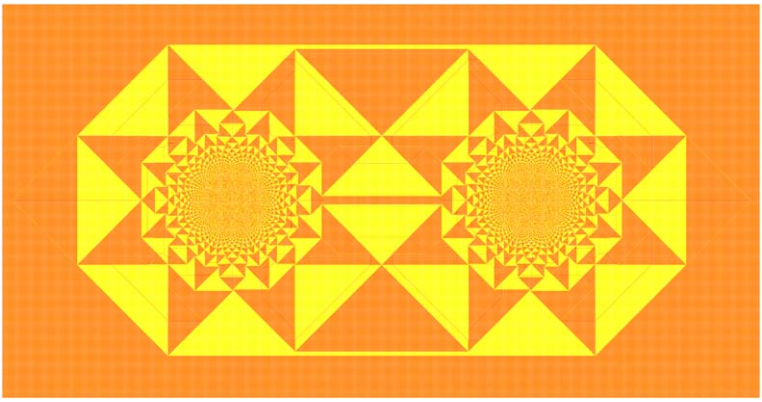

Fig. 9 (Color online) The pattern produced by adding $N = 640000$ grains each at $(-760, 0)$ and $(760, 0)$ on the F-lattice with the initial checkerboard distribution of grains and relaxing. This corresponds to $r_o = 0.95$. Color code *red* $= 0$ and *yellow* $= 1$. (Details can be seen in the online version using zoom in.)

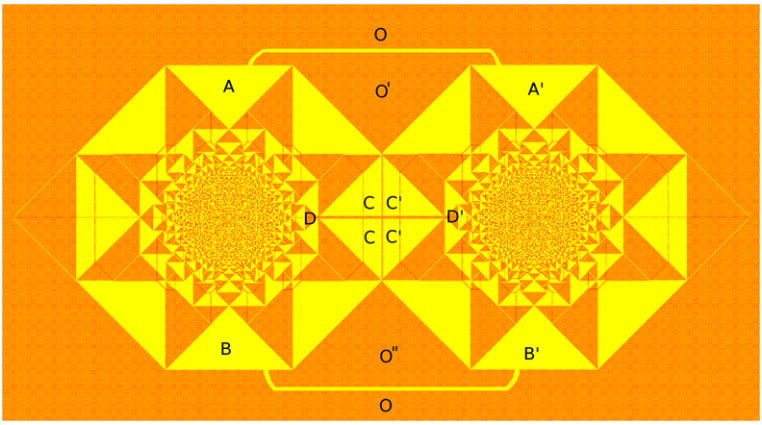

Fig. 10 (Color online) The pattern constructed by combining two single source patterns and drawing connecting lines between few patches following the connectivity in the pattern in Fig. 9

The pattern produced with two sources with $r_0 = 0.95$ is shown in Fig. 9. We see that there are still only two types of periodic patches, corresponding to $\Delta\rho(\mathbf{r})$ values 0 and $1/2$, and the slope of the boundaries between patches takes the values 0, ± 1 or ∞.

The relaxation due to overlap changes the adjacency graph from the case with no overlap. This modified adjacency graph, for r_o in the range 0.70 to 1.00, is shown in Fig. 12. For r_0 just below 1, these changes are few and are listed below.

(i) We note that the patches labelled A and A' in Fig. 10 have the same ξ and η dependence of the potential function ϕ. Then, for r_0 just below 1, these patterns can join with each other by a thin strip. This only requires a small movement in the boundaries of nearby patches (i.e. only a small change in the d and e values of nearby patches). Thus, in the adjacency graph, the vertices corresponding to A and A' are collapsed into a single vertex A in Fig. 12.

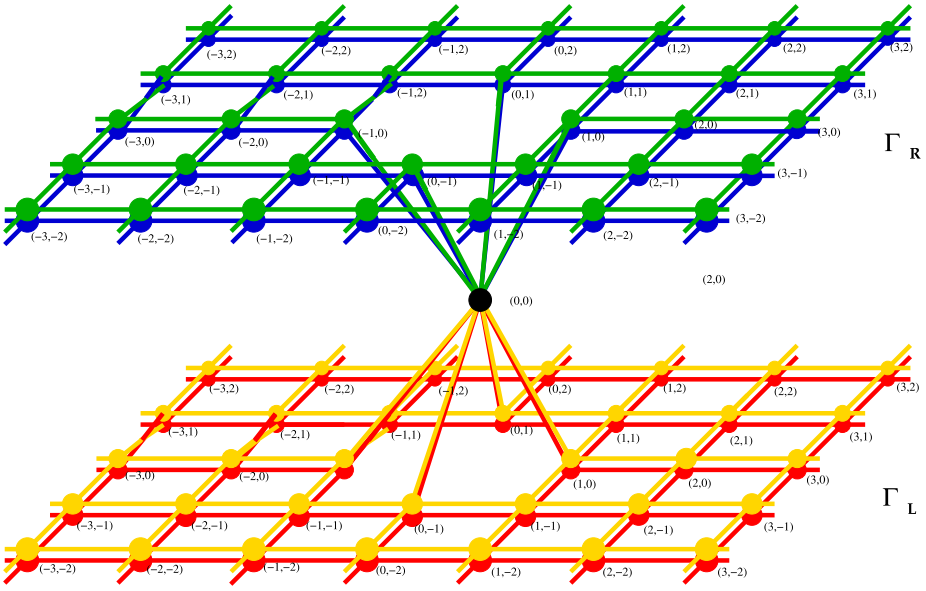

Fig. 11 (Color online) Representation of the adjacency graph of the patches for two non-overlapping single source patterns as a square grid on two Riemann surfaces each of two-sheets. The vertices with same (m, n) coordinates on different sheets are represented by different colors

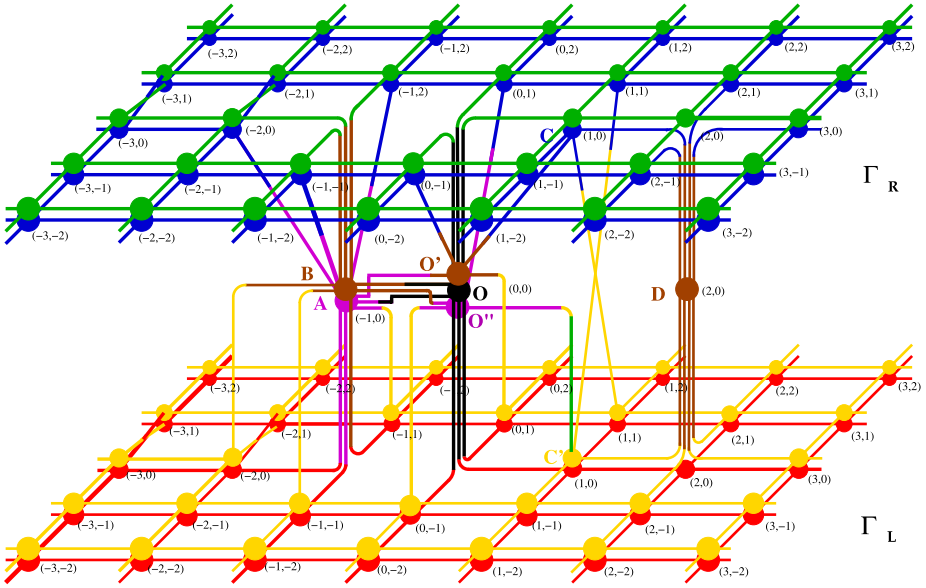

Fig. 12 (Color online) The adjacency graph for two intersecting single source patterns around two sites of addition placed at a distance $2\mathbf{r}_o$ from each other. The graph has the structure of square grids on four Riemann sheets except for a finite number of vertices indicated by the alphabet A, B, O, O', O'' and D shown placed in the middle layer. This graph remains unchanged for r_o in the range 0.70 to 1.00

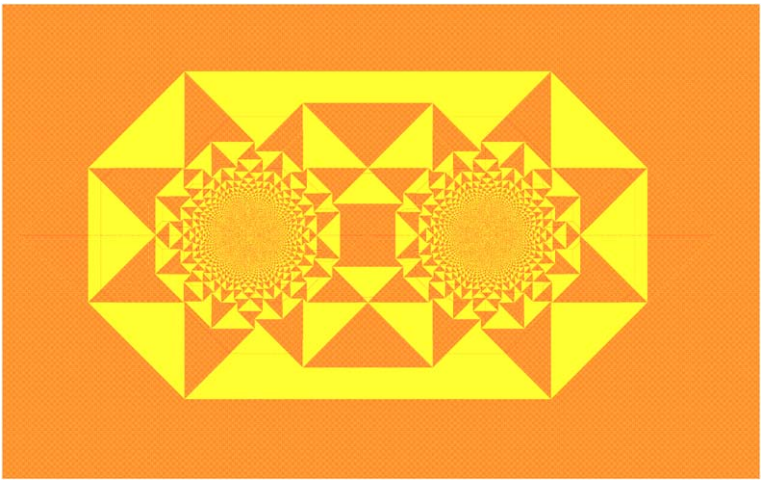

Fig. 13 (Color online) The pattern produced by adding 640000 grains at site $(-600, 0)$ and $(600, 0)$. Although the pattern is significantly different from the one in Fig. 9, their adjacency graph is same

(ii) Similarly, the vertices corresponding to the patches B and B' in Fig.10 are collapsed into a single vertex B in Fig. 12.

(iii) This divides the region outside the pattern in to three parts, O, O' and O''. They are also shown in Fig. 12 as separate vertices.

(iv) The patches marked C and C' also have the same quadratic form, and the vertical boundary between them disappears. However, the patches D and D' are also joined by a thin strip. This horizontal strip divides the joined C and C' into two again (Fig. 10).

The adjacency of other patches remains unchanged. The adjacency graph of the pattern is shown in Fig. 12. Interestingly, this new adjacency graph remains the same for all $0.70 < r_0 < 1$, even though for $r_o < 0.85$, the sizes of different patches are substantially different. Compare the pattern for $r_0 = 0.70$ in Fig. 13, with the pattern for $r_0 = 0.95$ in Fig. 9: The shape of the central patches in Fig. 13 is different from that in Fig. 9.

In Fig. 12, we have have placed the vertices which are formed by merging or dividing the patches, midway between the Riemann sheets corresponding to the two sources. As r_0 is decreased below 0.70, more collisions between the growing patches will occur and the number of vertices in this middle region will increase. For any nonzero r_0, the number of vertices in the middle layer is finite. In the $r_o \to 0$ limit, vertices from both the surfaces Γ_L and Γ_R come together and form a single Riemann surface corresponding to a single source pattern around $\mathbf{r} = 0$. For r_0 small, but greater than zero, the outer patches are arranged as in the single-source case, but closer to the sources, one has a crowded pattern near each source. In the adjacency graph, this corresponds to the vertices near the patch $(0, 0)$ roughly arranged as on a Riemann surface of two-sheets, while the ones farther from the patch $(0, 0)$ remain undisturbed on the 4-sheeted Riemann surface.

We now characterize the pattern with two sources and $r_0 > 0.70$ in detail by explicitly determining the potential function on this adjacency graph.

The Poisson equation analogous to (2) for this problem is

$$\nabla^2 \phi(\mathbf{r}) = \Delta\rho(\mathbf{r}) - \frac{N}{A^2}\delta(\mathbf{r} - \mathbf{r}_o) - \frac{N}{A^2}\delta(\mathbf{r} + \mathbf{r}_o). \tag{46}$$

Let us use the same quadratic form of the potential function given in (39) and (40).

Again using the same argument given in [6], it can be shown that m and n are the coordinates of the patches in both the adjacency graphs in Figs. 11 and 12. These coordinates are shown next to each vertex. Also, on this graph, the function $D(m,n) = d(m,n) + ie(m,n)$ satisfies the discrete Laplace equation

$$\sum_{m'}\sum_{n'} D(m',n') - 4D(m,n) = 0, \tag{47}$$

where (m',n') denote the neighbors of (m,n) in the odd or even sublattice [20]. Let us define $z_o = \xi_o + i\eta_o$ where (ξ_o, η_o) and $(-\xi_o, -\eta_o)$ are the coordinates corresponding to $\mathbf{r}_o$ and $-\mathbf{r}_o$. Considering that close to $\mathbf{r}_o$ and $-\mathbf{r}_o$ the potential $\phi(\mathbf{r})$ diverges logarithmically it can be shown (as done for single source pattern in [6]) that for large $|M|$,

$$\begin{aligned} D(m,n) &= \bar{z}_o \frac{M}{4} \pm \frac{A}{\sqrt{2\pi}}\sqrt{M} + \text{lower order in } M, \text{ on } \Gamma_L \\ &= -\bar{z}_o \frac{M}{4} \pm \frac{A}{\sqrt{2\pi}}\sqrt{M} + \text{lower order in } M, \text{ on } \Gamma_R, \end{aligned} \tag{48}$$

where A is a constant independent of N or Λ. The solution of (47) with the boundary condition $D(0,0) = 0$ and that in (48) for large $|M|$ determines the final pattern.

8 Numerical Analysis

In both the examples in Sects. 6 and 7 the patterns are characterized in terms of the solution of the standard two dimensional lattice Laplace equation on the corresponding adjacency graphs. The solution is well-known when $(m,n) \in \mathbb{Z}^2$ [21]. In our case where the lattice sites form surfaces of multiple sheets, we have not been able to find a closed-form expression for $D(m,n)$. However, the solutions can be determined numerically to very good precision by solving it on a finite grid $-L \le m,n \le L$ with the corresponding boundary conditions imposed exactly at the boundary.

For the pattern with the line sink, the calculation is performed with $D = M^{2/3}$ at the boundary and then the solution is normalized to have $d(1,0) = -1$. We determined d and e numerically for $L = 100$, 200, 300, 400 and 500 and extrapolated our results for $L \to \infty$. Comparison of the results from this numerical calculation and that obtained by measurements on the pattern is presented in Table 1. We consider the four different lengths R_1, R_2, R_3 and R_4 as defined in Fig. 14. By the definition of the diameter of the pattern $R_1 = 2\Lambda$. We present the values of R_2, R_3 and R_4 normalized by R_1 for different N. The asymptotic values of these lengths are determined from the values of d and e. Comparison of these results shows very good agreement between the theoretical and the measured values.

A similar numerical calculation is done for the pattern with two sources. In this case the boundary condition is given by (48). The value of A is determined from a self consistency condition that the diameter of the pattern in the reduced coordinate is 2 which

Table 1 Comparison of different lengths measured directly from the pattern in Fig. 14 for increasing values of N, with their theoretical values

N	896k	14336k	57344k	229376k	Theoretical
R_2/R_1	0.769	0.768	0.770	0.770	0.7698
R_3/R_1	0.675	0.675	0.667	0.668	0.6666
R_4/R_1	0.609	0.609	0.617	0.616	0.6172

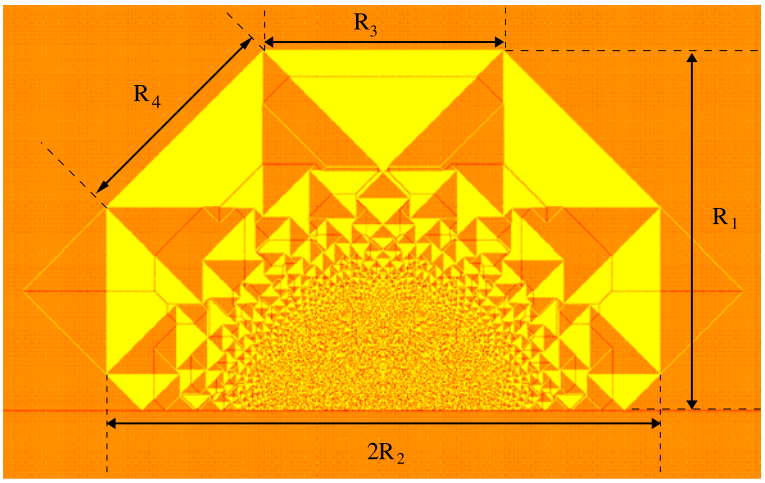

Fig. 14 (Color online) The spatial lengths R_1, R_2, R_3 and R_4 tabulated in Table 1

Table 2 Comparison of different lengths measured directly from the two source pattern for $r_o = 0.800$ with their theoretical values

N	2.5k	10k	40k	160k	640k	Theoretical
$R_1/\sqrt{N}$	1.84	1.84	1.84	1.83	1.83	1.82
$R_2/\sqrt{N}$	1.06	1.07	1.07	1.06	1.05	1.06
$R_3/\sqrt{N}$	0.22	0.21	0.20	0.19	0.18	0.18
$R_4/\sqrt{N}$	0.18	0.19	0.19	0.18	0.18	0.18
$R_5/\sqrt{N}$	0.20	0.22	0.21	0.21	0.21	0.21

imposes $2e(-1, 0) = -1$ corresponding to the vertex A in Fig. 12. We determined d and e numerically for $L = 100$, 200, 300, 400 and 500 and extrapolated our results for $L \to \infty$. A comparison of the results from this numerical calculation and that obtained by measurements on the pattern are presented in Table 2. We considered five different spatial lengths in the pattern, corresponding to $r_o = 0.800$. These different lengths are drawn in Fig. 15 and their values rescaled by $\sqrt{N}$, for the patterns with increasing N, are given in Table 2. The asymptotic values of these lengths are obtained using the values of d and e. The rescaled lengths extrapolated to the infinite N limit match very well with the theoretical results.

9 Discussion

While the results discussed have not been established rigorously, they can be considered as exact in the sense that the coordinates of all patches can be determined numerically to any desired precision by solving the Laplace equation. As noted before, it would be desirable to have a direct proof of the proportional growth property from the definition of the problem. Also, we use the observation that the asymptotic pattern consists of only two types of patches, and the adjacency graph of the pattern is also taken as observed. It would be nice to see it following from the definition of the problem. The unexpected accuracy of the scaling arguments giving (34), (36), (37), (38) also deserves to be understood better.

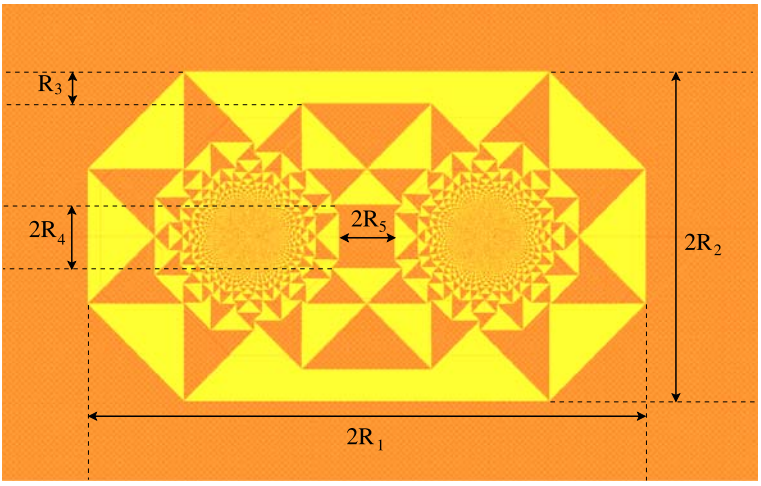

Fig. 15 (Color online) The spatial lengths R_1, R_2, R_3, R_4 and R_5 tabulated in Table 2

We have shown that the exact characterization of the patterns in the F-lattice on a checkerboard background reduces to solving a discrete Laplace equation on the adjacency graph of the pattern. For the single source pattern this graph is a square grid on a two-sheeted Riemann surface and in the presence of a line sink it is on a three-sheeted Riemann surface. This Riemann surface structure occurs for other sink geometries as well and the number of sheets can be determined from the way ϕ diverges near the origin.

If the potential $\phi(r)$ diverges as r^{-a} near the origin, then the corresponding complex function $\Phi(z) \sim z^{-a}$. Then $\frac{d^2}{dz^2}\Phi \sim z^{-2-a}$. In all the cases studied above, the patch to which point z belongs is characterized by integers (m, n), where $\frac{d^2}{dz^2}\Phi \sim m + in$. Also $\frac{d}{dz}\Phi \sim d + ie$. Writing $D = d + ie$, and $M = m + in$, we see that $D \sim M^{\frac{1+a}{2+a}}$. This then gives the number of Riemann sheets. For example, for the wedge angle $\omega = 2\pi$, we have $a = 1/2$. Then $D \sim M^{3/5}$, and the Riemann surface would have 5 sheets.

The patterns discussed so far in this paper have only two types of patches with densities $1/2$ and 1. But it is possible to have patterns with patches of other densities. For example, for the patterns with two sources, any finite inclination of the line joining the sources with the x-axis introduces patches which have areal density different from $1/2$ or 1. One such pattern produced by adding 40000 grains each at $(-180, 0)$ and $(180, 20)$ is shown in Fig. 16. The regions with stripes of red and yellow are patches of the new density. In addition, the boundaries of these patches have slopes other than 0, ± 1 and ∞. Most of the analysis presented here is applicable to this pattern, except that the matching conditions along the common boundary between two patches and the adjacency graph are different.

The cases in which the full pattern can be explicitly determined are clearly special. For example, one of the conditions used for the exact characterization of the patterns in this paper is that inside each patch the height variables are periodic and hence $\Delta\rho(\mathbf{r})$ is constant. It is easy to check that this condition is not met for most sink geometries. For example, patterns of the type discussed in Sect. 4 with any ω other than integer multiples of $\pi/4$ have aperiodic patches. In such cases, the present treatment for characterization of patterns is clearly not applicable. However, the scaling analysis for the growth of the spatial lengths in the pattern with N is still valid.

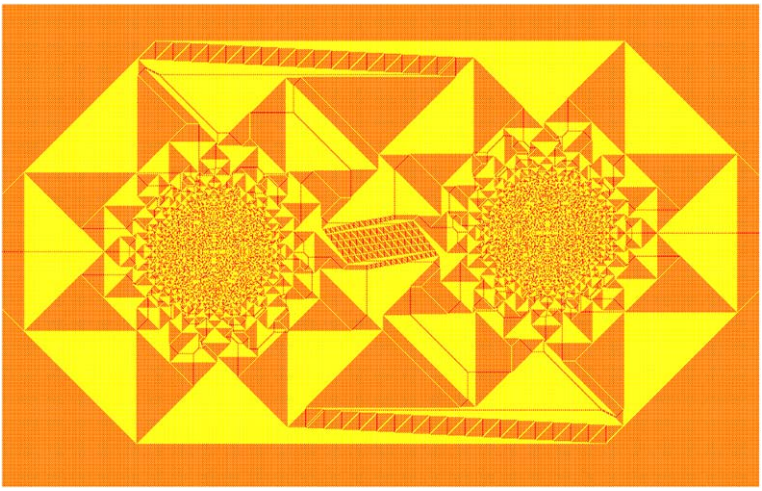

Fig. 16 (Color online) Pattern produced by adding $N = 40000$ grains each at $(-180, 0)$ and $(180, 20)$ on the F-lattice with initial checkerboard distribution of grains and relaxing. Color code *red* $= 0$ and *yellow* $= 1$. (Details can be seen in the online version using zoom in.)

The function $D = d + ie$ satisfies the discrete Cauchy-Riemann condition (see (41)). These functions are known as discrete holomorphic functions in the mathematics literature and in the context of critical two-dimensional lattice models [22]. Usually they have been studied for a square grid of points on the plane [20, 21]. While more general discretizations of the plane have been discussed [23, 24], not much is known about the behavior of such functions for multi-sheeted Riemann surfaces.

In our analysis we have also used the fact that the patterns have nonzero average overall excess density (i.e. C_2 in (10) is nonzero). The case $C_2 = 0$ is quite different, and requires a substantially different treatment. We hope to discuss such patterns in a future publication [25].

Acknowledgements We thank Prof. A. Libchaber for suggesting this problem and some useful discussions, and Prof. Ronald Dickman for critical reading of the manuscript. DD thanks the Department of Science and Technology, India for financial support through a J.C. Bose fellowship.

References

1. Schulman, L.S., Seidon, P.E.: Statistical mechanics of a dynamical system based on Conway's game of life. J. Stat. Phys. **19**, 293 (1978)
2. Pearson, J.E.: Complex patterns in a simple system. Science **261**, 189 (1993)
3. A particular mathematical model is discussed in Hadeler, K.P., Kuttler, C.: Dynamical models for granular matter. In: Granular Matter, vol. 2, pp. 9–18. Springer, Berlin (1999)
4. Falcone, M., Vita, S.F.: A finite-difference approximation of a two-layer system for growing sandpiles. SIAM J. Sci. Comput. **28**, 1120–1132 (2006)
5. Dhar, D.: Theoretical studies of self-organized criticality. Physica A **369**, 29–70 (2006)
6. Dhar, D., Sadhu, T., Chandra, S.: Pattern formation in growing sandpiles. Europhys. Lett. **85**, 48002 (2009)
7. Herrmann, H.J.: Geometrical cluster growth models and kinetic gelation. Phys. Rep. **136**, 153–224 (1986)
8. Liu, S.H., Kaplan, T., Gray, L.J.: Geometry and dynamics of deterministic sandpiles. Phys. Rev. A **42**, 3207–3212 (1990)

9. Dhar, D.: Studying self-organized criticality with exactly solved models (1999). arXiv:cond-mat/9909009
10. Borgne, Y.L., Rossin, D.: On the identity of sandpile group. Discrete Math. **256**, 775–790 (2002)
11. Boer, A.F., Redig, F.: Limiting shapes for deterministic centrally seeded growth models. J. Stat. Phys. **130**, 579–597 (2008)
12. Levine, L., Peres, Y.: Spherical asymptotics for the rotor-router model in $\mathbb{Z}^d$. Indiana Univ. Math. J. **57**, 431–450 (2008)
13. Ostojic, S.: Patterns formed by addition of sand grains to only one site of an Abelian sandpile. Physica A **318**, 187 (2003)
14. Ostojic, S.: Diploma thesis. Ecole Poly. Fed., Lausanne (2002) (unpublished)
15. Creutz, M.: Abelian sandpiles. Comput. Phys. **5**, 198–203 (1991)
16. Caracciolo, S., Paoletti, G., Sportiello, A.: Explicit characterization of the identity configuration in an Abelian sandpile model. J. Phys. A, Math. Theor. **41**, 495003 (2008)
17. Gravner, J., Quastel, J.: Internal DLA and the Stefan problem. Ann. Probab. **28**, 1528 (2000)
18. Levine, L., Peres, Y.: Scaling limit of internal aggregation models with multiple sources. Preprint (2009). arXiv:0712.3378v2
19. Duplantier, B., Saleur, H.: Exact surface and wedge exponents for polymers in two dimensions. Phys. Rev. Lett. **57**, 3179 (1986)
20. Cardy, J.: Discrete holomorphicity at two-dimensional critical points. J. Stat. Phys. (2009). doi:10.1007/s10955-009-9870-6
21. Duffin, R.J.: Basic properties of discrete analytic functions. J. Phys. A, Math. Theor. **41**, 495003 (2008)
22. Spitzer, F.: Principles of Random Walk, 2nd edn. Springer, Berlin (2001). Sec. 15, ch. 3
23. Mercat, C.: Discrete Riemann surfaces and the Ising model. Commun. Math. Phys. **218**, 177–216 (2001)
24. Lovász, L.: Discrete analytic functions: an exposition. In: Grigor'yan, A., Yau, S.-T. (eds.) Surveys in Differential Geometry. Eigenvalues of Laplacians and Other Geometric Operators, vol. IX. Int. Press, Somerville (2004)
25. Sadhu, T., Dhar, D.: Growing sandpile patterns on triangular lattice (in preparation)